1521-009X/12/4005-1024–1031$25.00
DRUG METABOLISM AND DISPOSITION
DMD 40:1024–1031, 2012

Vol. 40, No. 5
41616/3766481

Stereoselective Interaction of Pantoprazole with ABCG2. II. In Vitro Flux Analysis

Lipeng Wang, Markos Leggas, Philip E. Empey, and Patrick J. McNamara

Department of Pharmaceutical Sciences, College of Pharmacy, University of Kentucky, Lexington, Kentucky (L.W., M.L., P.J.M.); and Center for Clinical Pharmaceutical Sciences, School of Pharmacy, University of Pittsburgh, Pittsburgh, Pennsylvania (P.E.E.)

Received July 6, 2011; accepted February 21, 2012

ABSTRACT:

(−)Pantoprazole [(−)PAN] accumulated in rat milk stereoselectively, and this accumulation was attributed to rat Abcg2 (rAbcg2). In contrast, flux experiments at 25 μM showed that (+)pantoprazole [(+)PAN] was preferentially transported by rAbcg2. The purpose of the current study was to comprehensively evaluate the transport of PAN isomers in empty-Madin-Darby canine kidney II (MDCKII) and MDCKII cells expressing the human/rat (ABCG2/rAbcg2) isoforms at concentrations ranging from 3 to 200 μM. The apical-to-basolateral and basolateral-to-apical directional flux and the asymmetry efflux ratios were virtually identical for both isomers in empty (mock transfected)-MDCKII monolayers but were concentration dependent for both isomers in ABCG2 (human/rat)-MDCKII. Kinetic analysis using predicted cellular concentrations showed that (−)PAN had an 8-fold lower K_M compared with (+)PAN for both rAbcg2 (0.25 versus 1.85 μM) and ABCG2 (0.6 versus 5.32 μM). (+)PAN had a 3-fold higher T_{Max} compared with the (−)PAN for both rAbcg2 (7.86 versus 2.49 nmol/h · cm^2) and ABCG2 (10.2 versus 3.29 nmol/h · cm^2). Effective ABCG2 surface-area permeability of (−)PAN was 9920 and 5480 (μl/h)/cm^2 for rAbcg2 and ABCG2, respectively, compared with the (+)PAN isomer (4250 and 1920 μl/h · cm^2, respectively). These results indicate a stereoselective interaction of PAN with similar kinetic parameters for both human and rat ABCG2. (−)PAN is a better substrate than (+)PAN for ABCG2/rAbcg2 and provide a rationale for the preferential accumulation of (−)PAN into rat milk.

Introduction

Efflux transporters, such as ABCB1, ABCC2, and ABCG2, are localized in numerous tissues throughout the body and play important roles in drug absorption, distribution, metabolism, and excretion (Giacomini et al., 2010). These transporters can be major determinants of the pharmacokinetic, efficacy and safety profiles of drugs. Flux across a polarized cell monolayer, such as Caco-2 or Madin-Darby canine kidney II (MDCKII) cell line overexpressing transporters have become one of the more popular in vitro methods to characterize substrate-transporter interactions (Balimane et al., 2004; Balimane and Chong, 2005). However, a mechanistic understanding and quantitative description of transport or inhibition data from Transwell plates remains limited (Kalvass and Pollack, 2007; Sun and Pang, 2008).

ABCG2 is expressed on the apical surface of lactating mammary epithelial cells (Jonker et al., 2005) and facilitates the accumulation of substrate drugs in milk, including nitrofurantoin, cimetidine, topotecan, acyclovir, dietary carcinogens, ranitidine, and ciprofloxicin (Oo et al., 1995, 2001; McNamara et al., 1996; Gerk et al., 2001; Jonker et al., 2005; Merino et al., 2005, 2006; van Herwaarden et al., 2007; Vlaming et al., 2009). Although diffusion plays a major role in drug appearance in milk, ABCG2 clearly contributes to the accumulation of its substrates in milk. Pantoprazole (PAN) is an ABCG2 substrate, and yet, one clinical report indicated that it has a very low milk-to-serum (M/S) ratio (Plante et al., 2004). There is no clear rationale for such a low ratio for a good ABCG2 substrate.

PAN is marketed as a racemic mixture (Fig. 1), and differences in the overall disposition of the two isomers have been reported both in man (Tanaka et al., 2001) and in rats (Xie et al., 2005). In a companion article (Wang and McNamara, 2012), the disposition of PAN isomers in rat milk was explored and revealed a clear stereoselective difference associated with rat (rAbcg2). Milk-to-serum ratio of (−)PAN was 2.5-fold greater than that of (+)PAN, and the M/S of (−)PAN was affected to a greater degree by the administration of GF120918 [*N*-(4-[2-(1,2,3,4-tetrahydro-6,7-dimethoxy-2-isoquinolinyl)ethyl]-phenyl)-9,10-dihydro-5-methoxy-9-oxo-4-acridine carboxamide] than the M/S of (+)PAN. In contrast, in vitro experiments suggested that the rate of (+)PAN flux across a rAbcg2-MDCKII monolayer was greater than (−)PAN at a donor con-

This work was supported in part by the National Institutes of Health National Center for Research Resources [KL2-RR024154].

Article, publication date, and citation information can be found at http://dmd.aspetjournals.org.

http://dx.doi.org/10.1124/dmd.111.041616.

ABBREVIATIONS: MDCKII, Madin-Darby canine kidney II; ABCG2/Abcg2, ATP binding cassette transporter family G member 2; rAbcg2, rat Abcg2; PAN, pantoprazole; M/S, milk to serum; GF120918, *N*-(4-[2-(1,2,3,4-tetrahydro-6,7-dimethoxy-2-isoquinolinyl)ethyl]-phenyl)-9,10-dihydro-5-methoxy-9-oxo-4-acridine carboxamide; HPLC, high-performance liquid chromatography; P_{Obs}, observed permeability; PS_D, permeability-surface area for passive diffusion; PS_{PC}, permeability-surface area of paracellular transport; PS_{AE}, permeability-surface area of active efflux mediated by ABCG2 on apical side; ER_α, asymmetry efflux ratios; $PS_{AE,Eff}$, effective apical efflux permeability; B-to-A, basolateral-to-apical; A-to-B, apical-to-basolateral.

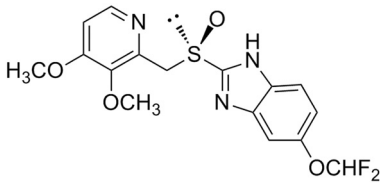

R-(+)

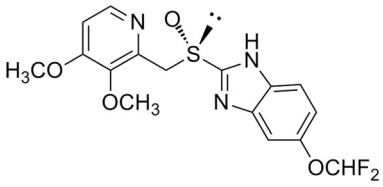

S-(-)

FIG. 1. The structure of PAN isomers.

centration of 25 μM, which is lower than the previously reported K_m estimated using Transwell flux experiments (Breedveld et al., 2004). The main purpose of this article is to fully explore this apparent contradiction by characterizing the transport of PAN isomers in monolayers consisting of rAbcg2 and human ABCG2 overexpressing MDCKII cells. The first objective was to describe differences in the interaction between PAN isomers and rAbcg2/ABCG2. The second objective was to examine any interspecies difference between rAbcg2 and ABCG2. In analysis of these data, a functional model was developed to quantify kinetic parameters for flux experiments involving an apical efflux pump.

Materials and Methods

Chemicals and Materials. PAN (pantoprazole) mixture (50:50) was purchased from Wyeth Pharmaceuticals Inc. (Princeton, NJ), and the isomers of PAN were a gift from Altana Pharma AG (Konstanz, Germany). Cell culture mediums were obtained from Invitrogen (Carlsbad, CA). All of the organic solvents [high-performance liquid chromatography (HPLC) grade] were purchased from Thermo Fisher Scientific (Waltham, MA), and all other chemicals were obtained from Sigma-Aldrich (St. Louis, MO) unless specified.

Overexpressing rAbcg2/ABCG2 in MDCK-II cell lines were used in the transport studies. The establishment of rat Abcg2 or empty vector (pcDNA3.1) alone in MDCKII was described previously (Wang et al., 2008). Human ABCG2 or empty vector (pcDNA3.1) alone in MDCKII was previously established in our laboratory. In brief, the pcDNA3.1 plasmid construct alone (empty vector) and the pcDNA3.1 plasmid containing wild-type ABCG2 were prepared for transfection. MDCKII cell transfection was performed at 50% confluence with the lipid-based FuGENE 6 transfection reagent at a 3:1 ratio per manufacturer's protocol. Transfected cells were then selected through the addition of 800 μg/ml G418 (Geneticin) to the parent cell line medium [minimal essential medium containing L-glutamine (GlutaMAX), 5% fetal bovine serum, 100 U/ml penicillin, and 100 μg/ml streptomycin]. Further selection and functional studies were performed by flow cytometry. The expression and localization of ABCG2 were confirmed by Western blot and confocal microscopy.

PAN Isomers Transport in Rat Abcg2 or Human ABCG2 in MDCKII Cells. In brief, rat/human ABCG2 or empty vector in MDCKII cells were seeded on microporous membrane filters (3.0-μm pore size, 24-mm diameter; Transwell 3414; Corning Life Sciences, Lowell, MA) at a density of 1.0×10^6 cells/well. Cells were grown for 4 days to achieve transepithelial electrical resistance $>200\ \Omega \cdot cm^2$, and medium was replaced every other day. Before the experiment, the medium at both the apical and basolateral side of the monolayer was replaced with 2 ml of Opti-MEM I medium (Invitrogen) without serum, and either apical or basolateral side was loaded with a 3, 10, 30, 50, and 200 μM concentration of individual PAN isomers and 0.2 μCi/ml [^{3}H]mannitol (PerkinElmer Life and Analytical Sciences, Waltham, MA). Cells were incubated at 37°C in 5% CO_2. Aliquots (50 μl) were collected to assess the paracellular flux of [^{3}H]mannitol into the opposite compartment; layers restricted mannitol transport to <1% of the total radioactivity per hour. For PAN isomer transport, 140-μl aliquots were taken at 0.5 and 1 h. Samples were stored at −80°C until the time of analysis by HPLC assay.

PAN Assay. Concentrations of PAN were assayed by HPLC (system) using a Luna RP18 125 × 4.0-mm column (Phenomenex, Torrance, CA), elution with 40% acetonitrile/60% 10 mM potassium phosphate buffer, pH 7.2, at 0.5 ml/min, and UV absorption at 290 nm. Aliquots of PAN in Opti-MEM I medium were directly injected onto the HPLC. The standard curve range was from 7.8 to 2000 ng/ml. All of the standard curves showed an intraday and interday variability of <10% and $r^2 > 0.999$.

Apparent Permeability. The observed permeability [P_{Obs}, (μl/h)/cm^2] of PAN isomers or paracellular marker was determined by calculating its initial transfer rate ($\Delta X/\Delta t$, picomoles per hour) across the cell layer and dividing by the surface area (A, cm^2) of the Transwell plate and the initial concentration (C_0, picomoles per milliliter) in the donor chamber (eq. 1). PAN isomers transport data in rat Abcg2 or human ABCG2 were expressed as mean ± S.D.

$$PS_{Obs} = \frac{\Delta X/\Delta t}{A \times C_0} \quad (1)$$

Theoretical and Mathematical Analysis. Assuming the substrate does not interact with endogenous transporters, passive diffusion permeability (PS_D) is the same across both basolateral and apical membranes; no cellular metabolism and rapid intracellular diffusion; a three-compartment kinetic model of transcellular flux across a monolayer system (ABCG2-MDCKII) is established in Fig. 2. In brief, the driving force for drug efflux from basolateral-to-apical side includes PS_D across both basolateral and apical membranes, paracellular transport (PS_{PC}) between cells, and active transport efflux on apical side (PS_{AE}) associated with the transporter. The model assumes that 1) the substrate does not interact with any endogenous transporters, 2) PS_D is the same across both membranes, and 3) there is rapid intracellular diffusion and no cellular metabolism. Substrate flux rates in three compartments can be described by the following set of differential equations (eqs. 2–4).

$$\frac{dX_B}{dt} = C_C(PS_D) - C_B(PS_D) + (C_A - C_B)PS_{PC} \quad (2)$$

$$\frac{dX_A}{dt} = C_C(PS_D + PS_{AE}) - C_A(PS_D) + (C_B - C_A)PS_{PC} \quad (3)$$

$$\frac{dX_C}{dt} = C_A(PS_D) + C_B(PS_D) - C_C(2PS_D + PS_{AE}) \quad (4)$$

where X_B, X_A, and X_C are the mass of drug in the basolateral, apical, and cellular compartment; C_C, C_B, and C_A are the concentration of drug in the cellular, basolateral, and apical compartment, respectively; PS_{AE}, PS_D, and PS_{PC} are the permeability-surface area products for active apical efflux, passive diffusion, and paracellular pathways, respectively.

Equations 2 and 3 can be further refined to describe the initial permeability-surface area product from basolateral-to-apical (B-to-A) ($PS_{Obs,B\to A}$) or apical-to-basolateral (A-to-B) ($PS_{Obs,A\to B}$)

$$PS_{Obs,B\to A} = \frac{\frac{dX_{A,B\to A}}{dt}}{C_B^0} = \left[\frac{(PS_D)(PS_D + PS_{AE})}{(2PS_D + PS_{AE})} + PS_{PC}\right] \quad (5)$$

$$PS_{Obs,A\to B} = \frac{\frac{dX_{B,A\to B}}{dt}}{C_A^0} = \frac{(PS_D)(PS_D)}{(2PS_D + PS_{AE})} + PS_{PC} \quad (6)$$

Paracellular permeability of mannitol was used as a surrogate for PAN PS_{PC}. PS_D was estimated from the PAN flux in parent MDCKII ($PS_{AE} = 0$) by rearranging eq. 5 or 6 as follows:

$$PS_D = 2[PS_{\text{or } Obs,A\to B}^{Obs,B\to A} - PS_{PC}] \quad (7)$$

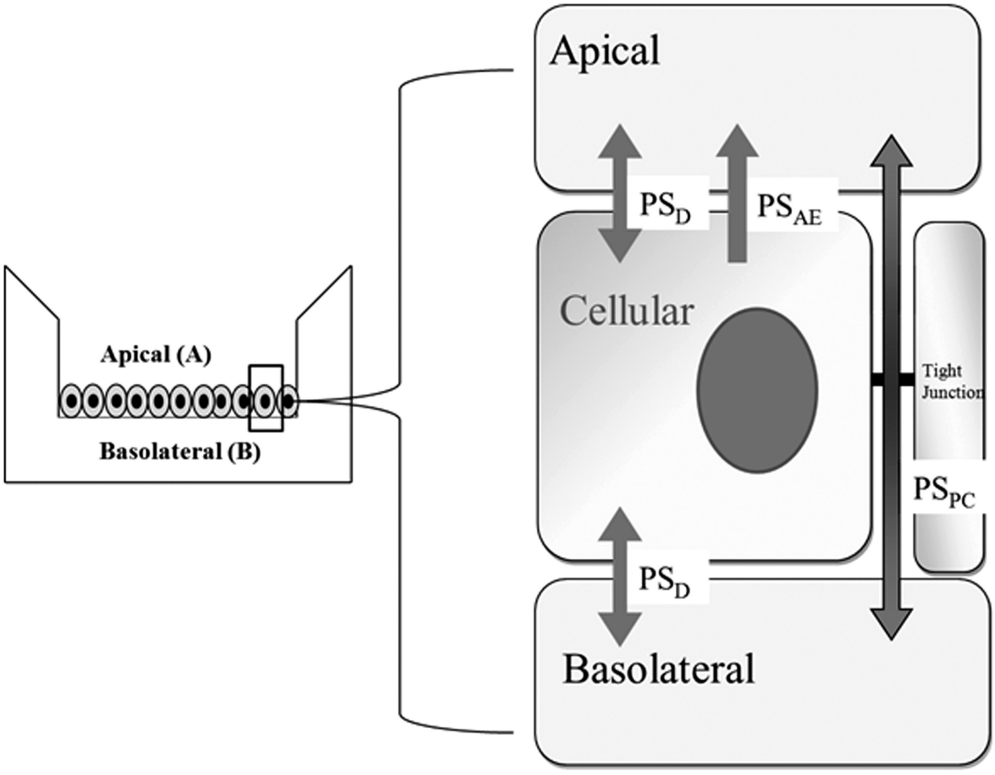

FIG. 2. Theoretical model of PAN flux across rAbcg2/ABCG2-MDCKII cell monolayer in a Transwell system.

PS_{AE} was estimated from B-to-A or A-to-B PAN flux in rAbcg2/ABCG2-MDCKII rearranging eq. 5 or 6 to yield eq. 8 or 9, respectively.

$$PS_{AE,B\to A} = \frac{PS_D{}^2 - 2PS_D(PS_{Obs,B\to A} - PS_{PC})}{((PS_{Obs,B\to A} - PS_{PC}) - PS_D)} \quad (8)$$

$$PS_{AE,A\to B} = \frac{PS_D{}^2 - 2PS_D(PS_{Obs,A\to B} - PS_{PC})}{(PS_{Obs,A\to B} - PS_{PC})} \quad (9)$$

Initial transfer flux of from B-to-A (assuming $C_A = 0$) can be rewritten (eq. 10) to estimate C_C.

$$C_C = \frac{C_B^0(PS_D)}{(2PS_D + PS_{AE})} \quad (10)$$

where PS_{AE} is approximated as in eqs. 8 and 9. Asymmetry efflux ratios (ER_α) is defined as the ratio of the initial rate of B-to-A flux divided by the initial rate of A-to-B (eq. 11).

$$ER_\alpha = \frac{\frac{dX_{Obs,B\to A}}{dt}}{\frac{dX_{Obs,A\to B}}{dt}} \quad (11)$$

Kinetic Parameter Estimation. The saturation transport kinetics of a drug efflux by rAbcg2 or ABCG2 at the apical surface can be modeled by eq. 12, where T_{max} is the maximum transport rate and K_M is the Michaelis constant. The PS_{Obs}, PS_D, and PS_{PC} of each PAN isomer were estimated experimentally and used to estimate PS_{AE} (eqs. 8 and 9). The intracellular concentrations (C_C) were estimated by eq. 10. Nonlinear regression using Prism 5.04 (GraphPad Software, Inc., San Diego, CA) was used to estimate K_M and T_{max}.

$$PS_{AE} = \frac{T_{Max}}{(K_M + C_C)} \quad (12)$$

An effective apical efflux permeability ($PS_{AE,Eff}$), observed when $C_C \ll K_M$ (similar to intrinsic clearance), would be defined as follows (eq. 13).

$$PS_{AE,Eff} = \frac{T_{Max}}{K_M} \quad (13)$$

Statistical Analysis. A multivariate analysis (SPSS, Chicago, IL; and IBM, White Plains, NY) was performed to assess the influence of concentration, direction, and isomer on PS_{Obs}. A sum-of-squares F-test of kinetic parameters (T_{Max} and K_M) was performed using Prism 5.04.

Results

Pantoprazole Isomers Transported in rAbcg2 or ABCG2. The overall flux of PAN isomers was evaluated for both rAbcg2 and ABCG2 to assess stereoselectivity and species differences. The expression level and functional viability of stably expressing rat Abcg2 (Wang et al., 2008) and human ABCG2 (Empey et al., 2006) cDNA or vector alone in MDCKII cell lines have been established previously. The mass transport of PAN isomers was studied in empty-MDCKII and rAbcg2-MDCKII cells as shown in Fig. 3. For both of the PAN isomers in empty-MDCKII monolayers, PS_{Obs} was slightly higher in the B-to-A direction and increasing with concentration ($P > 0.05$). In contrast, the transport of PAN isomers exhibited a strong directional flux in rAbcg2-MDCKII cell line. There were marked differences between the PAN isomers transport at 30 and 50 μM for both directions. At lower (3 and 10 μM) concentrations, the difference between the isomers became negligible. At the highest donor concentration (200 μM), the flux of both isomers was equivalent to that observed in the empty-MDCKII cells. Parallel results were observed in empty-MDCKII and human ABCG2-MDCKII cell line transport study (Fig. 4). The directional transport of the two isomers confirmed that PAN is a substrate for both rAbcg2 and ABCG2.

Permeability Parameters and Asymmetry Efflux Ratios. To ascribe specific membrane properties to individual isomers, the apparent permeability parameters (PS_{obs}, PS_D, and PS_{PC}) and ER_α (Tables 1 and 2) were obtained for both rAbcg2 and ABCG2.

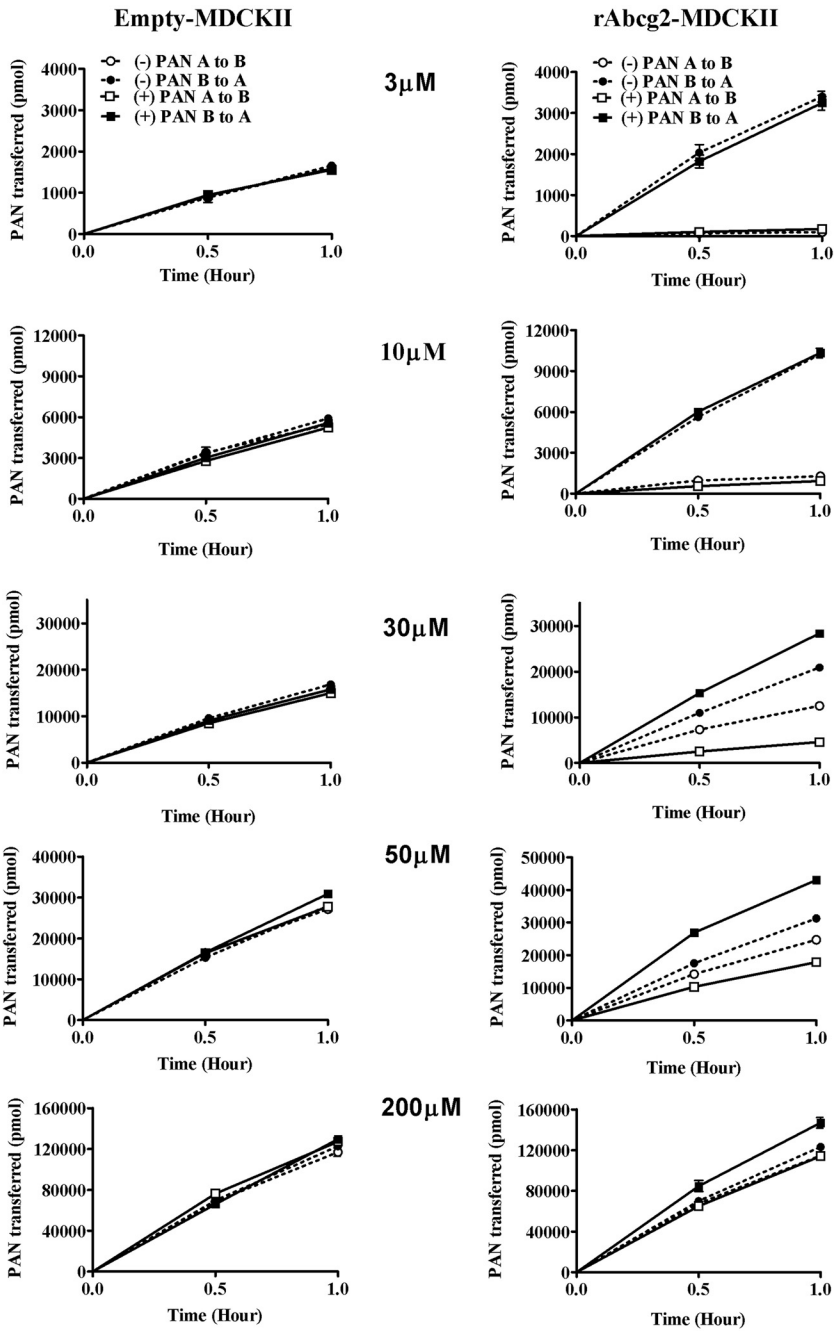

FIG. 3. Mean (±S.D., $n = 3$) PAN isomer transport in pcDNA3.1-MDCKII (left) or rAbcg2-MDCKII cells (right) at initial donor PAN concentrations of 3, 10, 30, 50, and 200 μM. The isomers were studied individually. Squares, (+)PAN; circles, (−)PAN; closed symbols, basolateral-to-apical flux; and open symbols, apical-to-basolateral flux.

Assuming that the transport permeability of mannitol is similar to PAN isomer transport across PS_{PC}, values were small and consistent across studies [range, 0.51–3.54 (μl/h)/cm^2]. PS_{PC} values were somewhat lower for ABCG2-MDCKII compared with empty-MDCKII. By use of PS_{obs} for PAN transport in empty-MDCKII, PS_D was estimated from eq. 7 at different concentrations and for both directions (Tables 1 and 2). The mean (±S.D.) PS_D values were 244 (±18) and 287 (±16) (μl/h)/cm^2 for the rat and human mock transfections, respectively.

PS_{obs} of PAN isomers in empty-MDCKII cell lines were similar for both directions at different concentrations resulting in ER_α values approximating unity for all of the experiments. By contrast, the PS_{obs} values of both PAN isomers in the transfected cell lines were markedly different with respect to direction, favoring strong basolateral-to-apical directional flux at the lower PAN concentration. The apparent flux were similar for the two isomers but with important differences. At the lowest PAN concentration, the ER_α of (−)PAN was nearly double that of (+)PAN for both Abcg2-MDCKII (Table 1) and ABCG2-MDCKII (Table 2). As donor concentration increased, PAN flux decreased for the basolateral-to-apical direction and increased for the apical-to-basolateral direction in Abcg2/ABCG2-MDCKII (Tables 1 and 2). As a result, the ER_α for both PAN isomers in both rat and human ABCG2-transfected cell lines decreased with increasing donor concentration until a value approaching unity was achieved (Tables 1 and 2).

Cellular Concentration Profile. Recognizing that the driving force of transport of an apical efflux transporter (i.e., Abcg2/ABCG2) is cellular and not donor concentration, simulated cellular concentrations of PAN isomers corresponding to donor concentrations (Fig. 5) were estimated using eq. 10 and based on initial estimates of perme-

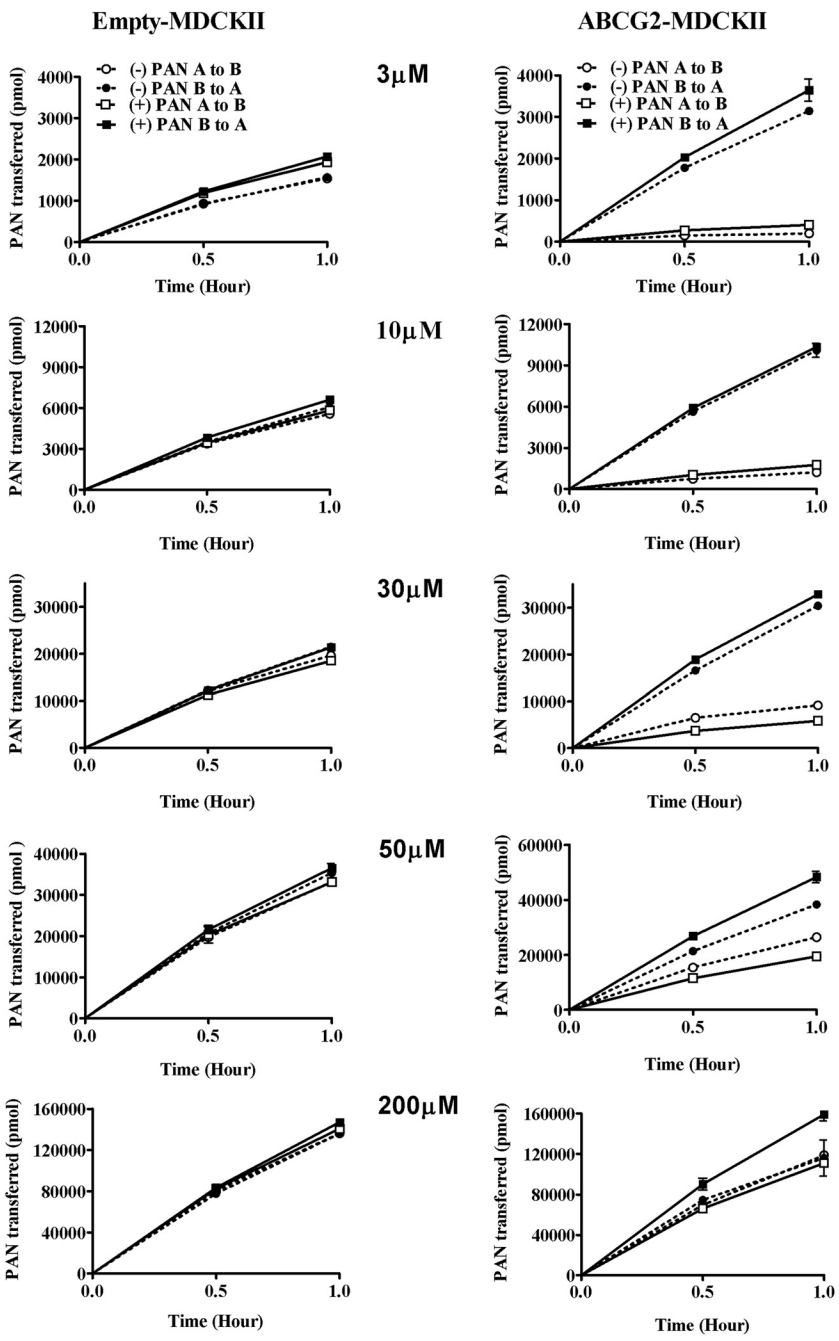

FIG. 4. Mean (±S.D., $n = 3$) PAN isomer transport in pcDNA3.1-MDCKII (left) or human ABCG2-MDCKII cells (right) at initial donor PAN concentrations of 3, 10, 30, 50, and 200 μM. The isomers were studied individually. Squares, (+)PAN; circles, (−)PAN; closed symbols, basolateral-to-apical flux; and open symbols, apical-to-basolateral flux.

ability parameters PS_{obs}, PS_D, and PS_{PC} (Tables 1 and 2) of PAN isomers and apparent PS_{AE} values (eqs. 8 and 9). At a low donor concentration (3 μM), cellular concentrations were estimated to be 3.2% of donor concentration for (−)PAN and 5.6% for (+)PAN for rAbcg2 and 5.5% for (−)PAN and 11% for (+)PAN for ABCG2. At a high donor concentration (above 50 μM), cellular concentration was predicted to approach half of the donor concentration (Fig. 5).

Kinetic Parameters K_M and T_{max} for Rat Abcg2 and Human ABCG2. To ascribe specific kinetic parameters for ABCG2/rAbcg2 for the individual isomers, the profile of apparent PS_{AE} (both directions) as a function of estimated cellular PAN concentration (Fig. 5) was analyzed as in Fig. 6. These estimates of PS_{AE} become less accurate as PS_{Obs} approaches its boundaries (very high or low donor concentrations). Kinetic parameters for the interaction of each isomer with Abcg2 and ABCG2 are shown in Table 3. The (−)isomer of PAN has an 8-fold lower K_M compared with the (+)PAN for both rAbcg2 (0.25 versus 1.85 μM, $P < 0.01$) and ABCG2 (0.6 versus 5.32 μM, $P < 0.01$), indicating a higher affinity of rAbcg2/ABCG2 for the (−)isomer. The (+)isomer of PAN has a roughly 3-fold higher T_{Max} compared with the (−)PAN for both rAbcg2 (7.86 versus 2.49 nmol/h · cm^2, $P < 0.01$) and ABCG2 (10.2 versus 3.29 nmol/h · cm^2, $P < 0.01$). rAbcg2 had a lower K_M (a higher affinity) for the PAN isomers compared with human ABCG2 but comparable T_{Max} values. The overall permeability associated with rAbcg2 and ABCG2 (PS_{AE}, effective transport clearance at low PAN concentrations) was calculated as the ratio of T_{Max} over K_M. PS_{AE} was twice that for the (−)PAN [9920 and 5480 (μl/h)/cm^2 for rAbcg2 and ABCG2, respectively] compared with the (+)PAN (4250 and 1920 μl/h · cm^2 for rAbcg2 and ABCG2, respectively).

TABLE 1

The observed ER_α, permeability parameters (PS_{PC}) of mannitol, and permeability parameters (PS_{obs} and PS_D) of PAN isomers transport in empty and rAbcg2-MDCKII as a function of PAN donor concentration

PS units are expressed as (μl/h)/cm^2.

Cell Line	Substrate/Isomer	Parameter	3 μM	10 μM	30 μM	50 μM	200 μM	Mean	S.D.
Empty-MDCKII	(−)PAN	PS_{obs} A→B	118	123	116	121	130	121	5
		PS_{obs} B→A	120	130	123	126	135	127	6
		ER_α	1.02	1.06	1.07	1.04	1.04	1.05	0.02
	(+)PAN	PS_{obs} A→B	116	114	110	123	142	121	13
		PS_{obs} B→A	117	121	116	135	140	126	11
		ER_α	1.01	1.07	1.06	1.09	0.98	1.04	0.05
	(−)/(+)PAN	PS_D	231	242	226	251	271	244	18
	Mannitol	PSpc	2.3	1.14	3.54	0.72	1.39	1.82	1.12
rAbcg2-MDCKII	(−)PAN	PS_{obs} A→B	7.4	30.1	92.5	109	127	N.A.	N.A.
		PS_{obs} B→A	253	224	151	137	136	N.A.	N.A.
		ER_α	34	7.44	1.63	1.26	1.07	N.A.	N.A.
	(+)PAN	PS_{obs} A→B	12.8	20.9	33.5	79.1	126	N.A.	N.A.
		PS_{obs} B→A	238	229	206	194	162	N.A.	N.A.
		ER_α	18.7	11	6.16	2.46	1.29	N.A.	N.A.
	Mannitol	PS_{PC}	0.51	0.88	3.44	0.72	1.59	1.43	1.2

N.A., not applicable.

Modeling Overall Permeability. To assess the validity of the deconvolution process, the overall PS_{Obs} was modeled as a function of donor concentration (Fig. 7) by using the PS_D values from the empty-MDCKII (Tables 1 and 2) as well as PS_{PC} from the transfected cell lines (Tables 1 and 2) and the ABCG2-related kinetic parameters (Table 3). The comprehensive relationships (eqs. 5 and 6) were effective in modeling PAN flux in both directions of (−)PAN ($r^2 = 0.979$) and (+)PAN ($r^2 = 0.988$) in ABCG2-MDCKII and (−)PAN ($r^2 = 0.985$) and (+)PAN ($r^2 = 0.986$) in rAbcg2-MDCKII.

Discussion

Our laboratory and others have demonstrated the importance of ABCG2 in drug accumulation in milk. In a companion article (Wang and McNamara, 2012), we examine the transfer of PAN into rat milk that clearly demonstrated ABCG2-associated accumulation of (−)PAN in milk; however, initial in vitro result showed that (+)PAN had greater transport than (−)PAN in Abcg2-MDCKII cell line at 25 μM. In current study, the flux of individual PAN isomers was examined at concentrations from 3 to 200 μM to more rigorously characterize the stereoselectivity of ABCG2.

PAN isomers have identical physiochemical properties; hence, diffusion properties of PAN isomers should be indistinguishable. The PS_D of PAN isomers transport in empty MDCKII cell line (parent cell line) at five different concentrations was virtually identical (Tables 1 and 2). There was essentially no directional transport difference observed, indicating limited interaction of PAN isomers with endogenous transporters in the parent MDCKII cell line. Consistent with the literature (Breedveld et al., 2004), both PAN isomers are substrates for rAbcg2/ABCG2. Moreover, both isomers display a concentration dependent flux profile in both human and rat ABCG2-MDCKII cell line (Figs. 3 and 4). The stereoselective interaction of PAN with rAbcg2/ABCG2 was clear at 30 and 50 μM but not evident at lower or higher concentrations.

The model (Fig. 2) provides a clear context for the interpretation of the isomer flux. At low concentrations, permeability across the apical membrane is so rapid (PS_{AE} is so large relative to PS_D) that the rate-limiting steps for PAN flux are associated with PS_D across the basolateral membrane and paracellular flux (PS_{PC}). Under these concentrations, overall flux becomes independent of rAbcg2/ABCG2 associated PS_{AE}. As rAbcg2/ABCG2 transport becomes saturated at higher concentrations (PS_{AE} is decreased), the contribution of diffu-

TABLE 2

The observed ER_α, permeability parameters (PS_{PC}) of mannitol and permeability parameters (PS_{obs} and PS_D) of PAN isomers transport in empty and ABCG2-MDCKII as a function of PAN donor concentration

PS units are expressed as (μl/h)/cm^2.

Cell Line	Substrate/Isomer	Parameter	3 μM	10 μM	30 μM	50 μM	200 μM	Mean	S.D.
Empty-MDCKII	(−)PAN	PS_{obs} A→B	126	143	140	137	152	140	9
		PS_{obs} B→A	128	155	150	146	151	146	11
		ER_α	1.01	1.08	1.08	1.06	0.99	1.04	0.04
	(+)PAN	PS_{obs} A→B	140	140	137	136	159	142	10
		PS_{obs} B→A	149	157	156	149	166	155	7
		ER_α	1.06	1.13	1.14	1.09	1.04	1.09	0.04
	(−)/(+)PAN	PS_D	267	291	289	277	309	287	16
	Mannitol	PSpc	2.3	3.29	1.22	3.44	2.29	2.51	0.9
rAbcg2-MDCKII	(−)PAN	PS_{obs} A→B	16.9	31.6	67.6	109	132	N.A.	N.A.
		PS_{obs} B→A	254	255	211	156	132	N.A.	N.A.
		ER_α	15	8.06	3.12	1.44	1	N.A.	N.A.
	(+)PAN	PS_{obs} A→B	30	42.2	43.6	79.6	126	N.A.	N.A.
		PS_{obs} B→A	258	246	240	195	179	N.A.	N.A.
		ER_α	8.61	5.81	5.5	2.45	1.42	N.A.	N.A.
	Mannitol	PS_{PC}	1	1.03	0.76	0.78	0.71	0.86	0.15

N.A., not applicable.

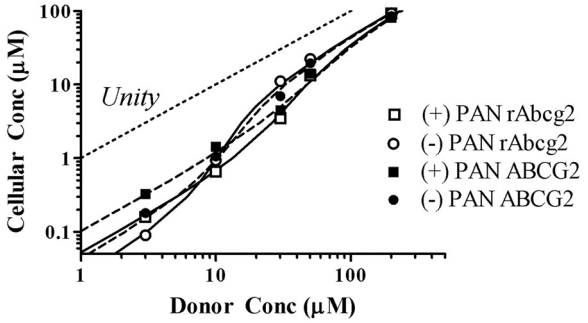

FIG. 5. Predicted cellular concentration of PAN (eq. 10) relative to donor concentration based on PS_D and PS_{PC} described in Tables 1 and 2 and approximated values of PS_{AE} (eqs. 8 and 9) were used. Squares, (+)PAN; circles, (−)PAN; open symbols, rAbcg2-MDCKII; closed symbols, ABCG2-MDCKII. The line of identity is provided as a reference.

sion across the apical membrane to overall flux approaches transport across empty-MDCKII. Only at the intermediate donor concentrations (Figs. 3 and 4) does the contribution and stereoselectivity of rAbcg2/ABCG2 to PAN transport become evident as measured by overall flux. Often flux studies, including those examining stereoisomer differences, are carried out at low substrate concentrations in high expressing clones to optimize the opportunity for detecting a response. Under such conditions, it is unlikely that stereoselective interactions would be reported since diffusion (i.e., across the opposite membrane or paracellular) is rate limiting and dominates the overall flux.

TABLE 3

The fitted mean (±S.E. from nonlinear fitting) kinetic parameters (K_m and T_{max}) in both rAbcg2 and ABCG2

Overall permeability associated with rAbcg2/ABCG2 was calculated as the ratio of T_{Max} over K_M.

Isoform	Parameters	(−)PAN	(+)PAN
		Mean (±S.E.)	
rAbcg2	T_{Max}, nmol/h · cm^2	2.49 ± 0.41	7.86 ± 2.20
	K_M, μM	0.25 ± 0.06	1.85 ± 0.66
	r^2	0.983	0.933
	$PS_{AE,Eff}$, (μ/h)/cm^2	9960	4250
ABCG2	T_{Max}, nmol/h · cm^2	3.29 ± 0.48	10.2 ± 2.43
	K_M, μM	0.59 ± 0.12	5.32 ± 1.62
	r^2	0.984	0.932
	$PS_{AE,Eff}$, (μ/h)/cm^2	5480	1920

Taken together, the flux data from empty and rAbcg2/ABCG2-MDCKII cell lines were consistent with the three compartment kinetic model shown in Fig. 2. The model comprises apparent permeability because of passive diffusion on either apical or basolateral side (PS_D), paracellular permeability through tight junction between cells (PS_{PC}), and ABCG2-mediated active transport permeability on the apical side (PS_{AE}). To analyze the data, several critical assumptions were made.

First, mannitol was assumed to be an adequate marker for PAN PS_{PC}. This assumption was particularly critical in establishing the limits of apical-to-basolateral flux at low PAN concentrations. Under

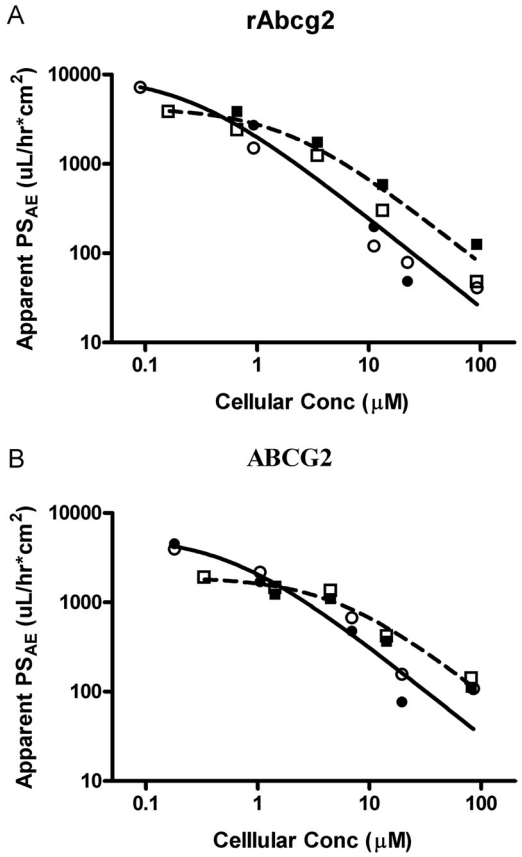

FIG. 6. PS_{AE} (eq. 12) as a function of simulated cellular PAN concentration (eq. 10). A, rAbcg2. B, human ABCG2-MDCKII cell monolayer. Squares indicate (+)PAN; circles, (−)PAN; open symbols, basolateral-to-apical PS_{AE}; and closed symbols, apical-to-basolateral PS_{AE}. The initial estimates of PS_{AE} (eqs. 8 and 9) were used to generate cellular concentration (eq. 10), and these concentrations were used in the final estimation process. Both axes were log-transformed for easier visualization; fitting was performed using untransformed pooled data from both directional PS_{AE}. The solid and dashed lines are the fitted results for the (−)PAN and (+)PAN isomers, respectively.

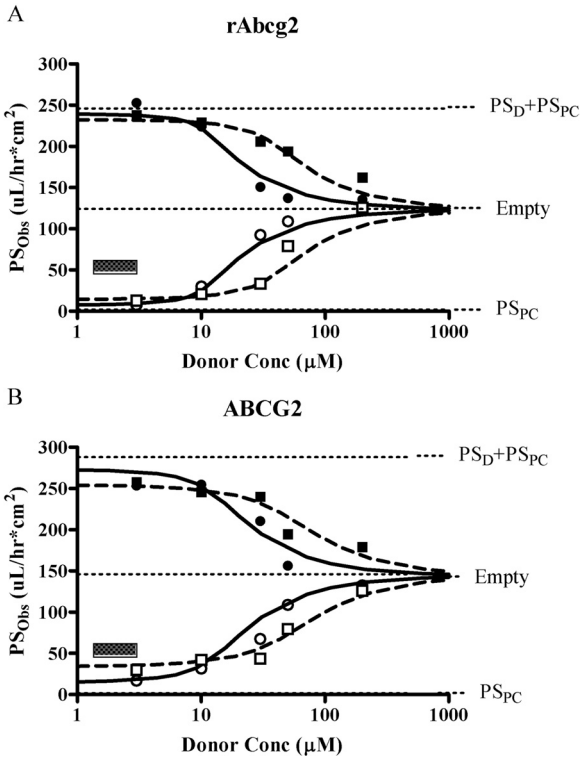

FIG. 7. PS_{obs} as a function of PAN donor concentration. A, rAbcg2. B, human ABCG2-MDCKII cell monolayer. Squares, (+)PAN; circles, (−)PAN; closed symbols, basolateral-to-apical flux; and open symbols, apical-to-basolateral flux. The simulation line represents eqs. 5 and 6 for basolateral-to-apical and apical-to-basolateral flux, respectively. Fitted parameters T_{MAX} and K_M (Table 3) were used to generate cellular concentration (eq. 10) and simulation of overall PS_{obs} together with PS_D and PS_{PC} as described in Tables 1 and 2. Model limits for basolateral-to-apical (PS_D + PS_{PC}), apical-to-basolateral (PS_{PC}), and empty cell line flux are presented for reference points. The small square box presents the range of PAN concentration in serum in rat or pharmacological concentration in human, respectively.

low substrate concentrations in high expressing clones, good substrates can have PS_{AE} values that are very large (e.g., $PS_{AE} > 10 \cdot PS_D$ as is the case for PAN). In practical terms, most of the substrate that enters the cell from the apical side is fluxed back out to the donor compartment, and more of the drug reaching the basolateral side is associated with PS_{PC}.

The second assumption was related to the estimation of cellular concentration. Ideally, intracellular unbound concentrations should be measured; however, this is technically very challenging. Relating kinetic parameters V_{Max} and K_M to donor concentrations was problematic. Initial attempts to fit flux to permutations of the Michaelis-Menten equation as a function of donor concentration resulted in fits that did not mimic the observed data. Fitting flux to donor concentrations suggested an apparent cooperative interaction (i.e., Hill coefficient) with the transporter (Pan et al., 2007). The driving force for an apical efflux transporter, such as rAbcg2/ABCG2, is cellular and not donor concentration. The apparent cooperativity reflected the fact that there is relatively more cellular drug concentration as donor concentration increases because of saturation of the efflux transporter (Fig. 5). Intracellular concentrations were not measured in the current study but were predicted by the model (Fig. 2) using the apparent PS_{AE} as well as estimates of PS_D and PS_{PC}.

These intracellular concentrations were then used to estimate kinetic parameters. The estimated K_M values ranged from 0.25 to 5.3 μM, whereas the donor concentrations around the donor concentration necessary to achieve these concentrations (Fig. 7) were in the 20 to 100 μM range. The (−)PAN had a K_M value that was 8-fold lower of the (+)isomer, indicating that (−)PAN had an 8-fold higher affinity for ABCG2 as well as rAbcg2. The capacity (T_{Max}) was 70% lower for (−)PAN for ABCG2 and rAbcg2. For typical therapeutic dosing, serum unbound concentrations are likely to be below 0.1 μM; hence, cellular concentrations would also be expected to be well below the K_M. The $PS_{AE,Eff}$ (listed in Table 3) would be more than 2-fold greater for (−)PAN compared with the (+)isomer. Therefore, (−)PAN is predicted to be a better substrate for rAbcg2/ABCG2 than (+)PAN. In the companion article (Wang and McNamara, 2012), the M/S for (−)PAN in rats was 1.36 and decreased markedly in response to GF120918 (an inhibitor of rAbcg2/ABCG2) compared with 0.54 for (+)PAN. Hence, the stereoselective effect of PAN with rAbcg2 in vitro manifested itself in a measureable in vivo difference in disposition, i.e., accumulation in rat milk.

Isolating the various parameters (PS_D, PS_{PC}, T_{Max}, and K_M) allowed the overall PS_{Obs} to be successfully modeled (Fig. 7). PAN flux in the B-to-A direction at a low PAN concentration was very rapid across the apical membrane, and overall flux was limited by the rate of diffusional flux across the basolateral membrane plus diffusion via the paracellular pathway. PAN flux in the A-to-B direction was limited largely to paracellular diffusion because the counter flux associated with PS_{AE} was so efficient that virtually none of the drug which entered the cell from the apical surface fluxed to the basolateral compartment through the cell itself.

The current in vitro flux data for PAN isomers would suggest that the stereoselectivity in rat milk accumulation (Wang and McNamara, 2012) would also hold for human exposure as well because ABCG2 was 2-fold difference in $PS_{AE,Eff}$ for PAN isomers (Table 3). The one case report did not examine individual isomers (Plante et al., 2004). The current work did not provide insights into the observed clinical report of a low M/S for pantoprazole (Plante et al., 2004).

In conclusion, there was stereoselective transport of PAN isomers in monolayers of both rAbcg2 and human ABCG2 expressed in MDCKII cell line with the (−)isomer possessing a greater affinity. A mechanism based model was used to quantify differences in kinetic parameters between the two isomers, which were not evident by examining flux at any single concentration. The unique characteristic of PAN isomers interaction with ABCG2 provided ideal experimental evidence to model drug transport across a cell monolayer. These kinetic parameters also provided insights to the extent of differences that arise for in vivo studies. The current work also provided insights into the species difference in ABCG2 transport.

Authorship Contributions

Participated in research design: Wang and McNamara.

Conducted experiments: Wang.

Contributed new reagents or analytic tools: Wang.

Performed data analysis: Wang and McNamara.

Wrote or contributed to the writing of the manuscript: Wang, Leggas, Empey, and McNamara.

References

Balimane PV and Chong S (2005) A combined cell based approach to identify P-glycoprotein substrates and inhibitors in a single assay. *Int J Pharm* **301:**80–88.

Balimane PV, Patel K, Marino A, and Chong S (2004) Utility of 96 well Caco-2 cell system for increased throughput of P-gp screening in drug discovery. *Eur J Pharm Biopharm* **58:**99–105.

Breedveld P, Zelcer N, Pluim D, Sönmezer O, Tibben MM, Beijnen JH, Schinkel AH, van Tellingen O, Borst P, and Schellens JH (2004) Mechanism of the pharmacokinetic interaction between methotrexate and benzimidazoles: potential role for breast cancer resistance protein in clinical drug-drug interactions. *Cancer Res* **64:**5804–5811.

Empey PE, Leggas M, and McNamara PJ (2006) PhIP transport in ABCG2 stably transfected MDCKII cells. *American Association of Pharmaceutical Scientists Meeting*; 2006 Nov 1; San Antonio, TX. AAPS PharmSci 8(S2), Abstract W5320.

Gerk PM, Kuhn RJ, Desai NS, and McNamara PJ (2001) Active transport of nitrofurantoin into human milk. *Pharmacotherapy* **21:**669–675.

Giacomini KM, Huang SM, Tweedie DJ, Benet LZ, Brouwer KL, Chu X, Dahlin A, Evers R, Fischer V, Hillgren KM, et al. (2010) Membrane transporters in drug development. *Nat Rev Drug Discov* **9:**215–236.

Jonker JW, Merino G, Musters S, van Herwaarden AE, Bolscher E, Wagenaar E, Mesman E, Dale TC, and Schinkel AH (2005) The breast cancer resistance protein BCRP (ABCG2) concentrates drugs and carcinogenic xenotoxins into milk. *Nat Med* **11:**127–129.

Kalvass JC and Pollack GM (2007) Kinetic considerations for the quantitative assessment of efflux activity and inhibition: implications for understanding and predicting the effects of efflux inhibition. *Pharm Res* **24:**265–276.

McNamara PJ, Meece JA, and Paxton E (1996) Active transport of cimetidine and ranitidine into the milk of Sprague Dawley rats. *J Pharmacol Exp Ther* **277:**1615–1621.

Merino G, Alvarez AI, Pulido MM, Molina AJ, Schinkel AH, and Prieto JG (2006) Breast cancer resistance protein (BCRP/ABCG2) transports fluoroquinolone antibiotics and affects their oral availability, pharmacokinetics, and milk secretion. *Drug Metab Dispos* **34:**690–695.

Merino G, Jonker JW, Wagenaar E, Pulido MM, Molina AJ, Alvarez AI, and Schinkel AH (2005) Transport of anthelmintic benzimidazole drugs by breast cancer resistance protein (BCRP/ABCG2). *Drug Metab Dispos* **33:**614–618.

Oo CY, Kuhn RJ, Desai N, and McNamara PJ (1995) Active transport of cimetidine into human milk. *Clin Pharmacol Ther* **58:**548–555.

Oo CY, Paxton EW, and McNamara PJ (2001) Active transport of nitrofurantoin into rat milk. *Adv Exp Med Biol* **501:**547–552.

Pan G, Giri N, and Elmquist WF (2007) Abcg2/Bcrp1 mediates the polarized transport of antiretroviral nucleosides abacavir and zidovudine. *Drug Metab Dispos* **35:**1165–1173.

Plante L, Ferron GM, Unruh M, and Mayer PR (2004) Excretion of pantoprazole in human breast. *J Reprod Med* **49:**825–827.

Sun H and Pang KS (2008) Permeability, transport, and metabolism of solutes in Caco-2 cell monolayers: a theoretical study. *Drug Metab Dispos* **36:**102–123.

Tanaka M, Ohkubo T, Otani K, Suzuki A, Kaneko S, Sugawara K, Ryokawa Y, and Ishizaki T (2001) Stereoselective pharmacokinetics of pantoprazole, a proton pump inhibitor, in extensive and poor metabolizers of S-mephenytoin. *Clin Pharmacol Ther* **69:**108–113.

van Herwaarden AE, Wagenaar E, Merino G, Jonker JW, Rosing H, Beijnen JH, and Schinkel AH (2007) Multidrug transporter ABCG2/breast cancer resistance protein secretes riboflavin (vitamin B2) into milk. *Mol Cell Biol* **27:**1247–1253.

Vlaming ML, Lagas JS, and Schinkel AH (2009) Physiological and pharmacological roles of ABCG2 (BCRP): recent findings in Abcg2 knockout mice. *Adv Drug Deliv Rev* **61:**14–25.

Wang L, Leggas M, Goswami M, Empey PE, and McNamara PJ (2008) *N*-(4-[2-(1,2,3,4-Tetrahydro-6,7-dimethoxy-2-isoquinolinyl)ethyl]-phenyl)-9,10-dihydro-5-methoxy-9-oxo-4-acridine carboxamide (GF120918) as a chemical ATP-binding cassette transporter family G member 2 (Abcg2) knockout model to study nitrofurantoin transfer into milk. *Drug Metab Dispos* **36:**2591–2596.

Wang L and McNamara PJ (2012) Stereoselective Interaction of Pantoprazole with ABCG2. I. Drug accumulation in rat milk. *Drug Metab Dispos* **40:**1018–1023.

Xie Z, Zhang Y, Xu H, and Zhong D (2005) Pharmacokinetic differences between pantoprazole enantiomers in rats. *Pharm Res* **22:**1678–1684.

Address correspondence to: Dr. Patrick J. McNamara, Department of Pharmaceutical Sciences, College of Pharmacy, University of Kentucky, 789 South Limestone, Lexington, Kentucky 40536. E-mail: pmcnamar@email.uky.edu